

## CHAPTER 37

### COMPUTER AID FOR OPTIMUM DESIGN OF TSUNAMI WAVES

Toshio Iwasaki  
Professor of Tohoku University

#### Abstract

The tsunami process of their generation and propagation to the near-coast offshore region is discussed. Purpose is to give optimum configurations of tsunami waves of large magnitude, which can be used as boundary conditions for the analysis of the dynamic process near the shore or around structures in coastal zone.

They are obtained by numerical computations along the southern coast of the Hokkaido and the Sanriku Coast for various tsunami sources set on the continental shelf facing to the Japan Submarine Trench. Dispersive nature of the tsunamis seems to make the problem very complicated. However statistical results thus obtained can be accepted for the base of design of structures.

#### INTRODUCTION

In 1933 a large tsunami had attacked the Sanriku Coast. Since then construction of counter measures against tsunami has been continued there, which was accelerated by the experience of the Chilean Earthquake Tsunami in 1960. Now in 1974, almost all lowland areas are protected by sea walls, revetments and dikes. Design method used for such structures was conventional such that their height was determined by maximum traces of the inundation of some peculiar tsunami selected from past records with or without some margin. This method seems to follow the technique of the river engineering for the design of river embankments. However flow direction against their horizontal alignment are completely different. So their functions against tsunamis are doubtful if many dynamic phenomena such as harbour resonance, shoaling, runup and overtopping are not examined.

Basically, tsunami waves are generated by the sea bottom dislocation in consequence of underwater earthquake and are considered as transient waves. Especially the source regions of tsunamis which attacked the Japan Islands were ordinally at the western slope of the Japan Submarine Trench and the distance to the coast was nearly the same order of the breadth of the source. Consequently tsunamis are still in the dispersive process even at the coastline. Moreover these waves are transformed by reflection and refraction superposed by the shelf resonance and the edge waves. So that it is extremely difficult to estimate the tsunami wave configurations for analysis of dynamic nature when intruding the coastal area.

Thus the tsunami process can be divided into two, one is the process of generation and propagation to the region such as harbour entrance or just off the coastal beach, where the depth is about 100 or 200 meters, say. We call this region near-coast offshore region. The other is the process nearer than this region.

This paper concerns to the former. Purpose is to give optimum

configurations of tsunami waves in the near-coast offshore region which will make possible the analysis of the second process for the design of structures against tsunamis. Firstly the idea of designed tsunami was proposed. Then the dimensions of the source areas were calculated, which enabled to construct the mathematical models for several kinds of tsunami magnitude and source locations.

DESIGNED TSUNAMI

K. Iida had published historical records of tsunamigenetic earthquakes during 1868 and 1962 as shown in Table 1.<sup>(1)</sup> Up to date, selected tsunamis for the design of protection works on the Sanriku Coast were the Sanriku Large Tsunami in 1933 and the Chilean Earthquake Tsunami in 1960 which

Table 1

Maximum Run-up	Japan			Sanriku Coast			Magnitude m
	Numbers of generation	Summation	Average return period	Numbers of generation	Summation	Average return period	
0.0 - 0.63 <sup>m</sup>	37	84	1.1	21	44	2.1	-1
0.63- 1.25	24	47	2.0	11	23	4.4	
1.25- 2.50	10	23	4.1	5	12	7.8	0
2.5 - 5.00	6	13	7.2	3	7	13.4	1
5.0 -10.0	4	7	13.4	2	4	23.1	2
10.0 -20.0	1	3	31.3	0	2	47.6	3
20.0-40.0	2	2	47.6	2	2	47.6	4

magnitudes proposed by Imamura were both 3. This recurrence interval is 31.3 years in Japan and 47.6 years in the Sanriku Coast as shown in Table 1. As such recurrence interval is considered as proper by river engineers, it may be chosen also for the standard design of tsunami structures. Then budget balance of the amount of investments against the benefit may become possible.

THE SOURCE AREAS OF THE TSUNAMIS

The wave sources are usually assumed as elliptic which dimensions can be estimated by the following equations.

$$m=2.61 M - 18.44 \tag{1}$$

$$M=6.27 + 0.76 \log_{10} \ell \tag{2}$$

$$\epsilon = \tanh \left[ 1.5 \tanh \left( \left( \frac{\pi}{2012} \right)^{1/2} \cdot \ell^{2/3} \right) \right] \tag{3}$$

$$2a = \ell / \epsilon \tag{4}$$

$$2b = \ell \cdot (1 - \epsilon^2)^{1/2} / \epsilon \tag{5}$$

$$S = \pi ab \tag{6}$$

$$\log_{10} E_t = 0.6m + 11.4 - \log_{10} 9.8 \tag{7}$$

m and M are the magnitudes of the tsunami and the earthquake respectively.

$\epsilon$ ,  $\ell$ ,  $a$ ,  $b$ ,  $S$  are the eccentricity, the distance between foci in km, the half length of the major axis in km, that of the minor axis in km and the area of the source in square km respectively. And  $E_t$  is the tsunami energy in ton-meter units.

Such ellipse has been proposed by Iida as the aftershock area of earthquake. However Dr. T. Hatori analysed all tsunami records around Japan during 1959 and 1968 using the adverse refraction diagrams and concluded that aftershock area was roughly equal to tsunami source area.<sup>(2)</sup> This is checked here in fig.1 where the relationship between  $\ell$  and  $M$  is shown. Full circles were obtained from the wave source ellipses obtained by Hatori including other materials since 1929. Iida (1959)<sup>(3)</sup> and Wilson (1962)<sup>(4)</sup> proposed empirical equations for aftershock areas. It can be said that wave sources are usually larger than aftershock areas. However the discrepancy of these equations from the data gives overestimate around  $M$  of 8.0 which is the most important magnitude for the design purpose. So the relationship is adjusted as given in Eq. (2).

Fig. 2 shows the relationship between the eccentricity  $\epsilon$  and  $\ell$  in which full circles are plotted again from Hatori's data. Data are scattered. However Eq.(3) which was presented by Wilson may be used successfully to represent this relationship.

Eq.(1) represents the relationship between tsunami and earthquake magnitudes  $m$  and  $M$  proposed by Iida and is used in general. And also the relations between tsunami magnitude  $m$  and tsunami energy  $E_t$  (erg) are shown in fig.3 where full circles are obtained from various literatures given by Japanese scientists. The straight line shows Eq.(7) given by Dr. R. Takahashi (1950) which expresses average values although data are remarkably scattered.<sup>(5)</sup>

Regional pattern of the sea bottom movement is most difficult to estimate as depth is over two thousand meters and there are many hypothesis about it. For example, one model is given such that the longer axis as a fault line and the linear distribution of the bed displacement from zero at the edges to some extent at the fault line which are upheaval on one side and downthrust on the other side. Other models are given by optimum estimation to realize the most favourable wave height distribution along coasts for actual records by numerical tests. However a simple uniform distribution of upheaval is used here tentatively, which is given by the following equation.

$$\eta_{\max} = \sqrt{\frac{2E_t}{w_0 S}} \quad (8)$$

$\eta_{\max}$  is the maximum dislocation and  $w_0$  is the unit weight of the sea water. The time history is assumed as linear.

Using equations of (1) to (8), dimensions of tsunami sources and the amount of upheaval are calculated for various magnitudes of earthquake or tsunami. Table 2 shows three examples which are used for mathematical models in the following.

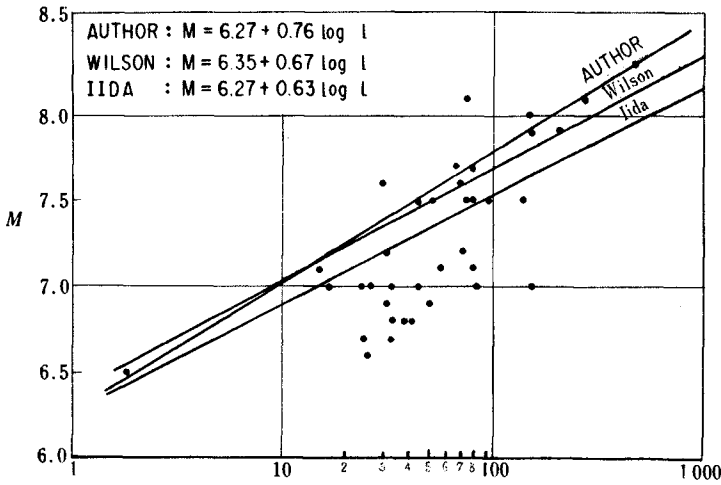


Fig.1. Relationship of Earthquake Magnitude  $M$  to the Distance between Foci.

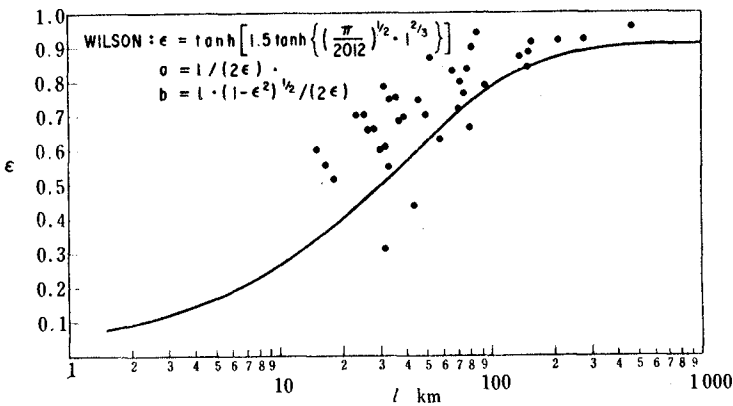


Fig.2 Relationship of Eccentricity of Source Region to the Distance between Foci.

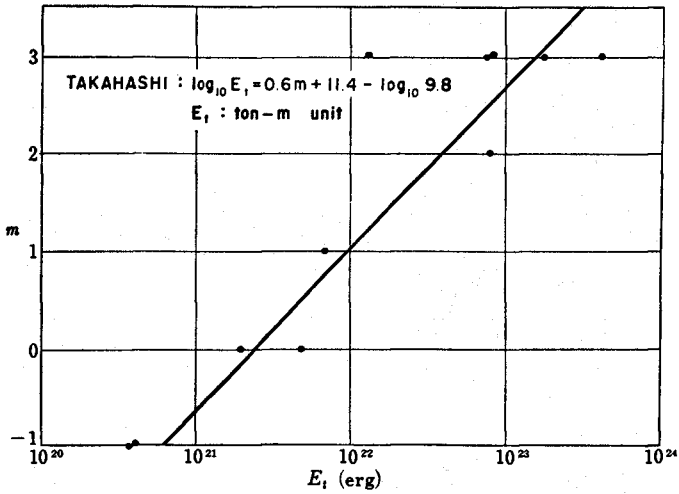


Fig.3 Relationship of Earthquake Energy  $E_t$  (erg) to Tsunami Magnitude  $m$ .

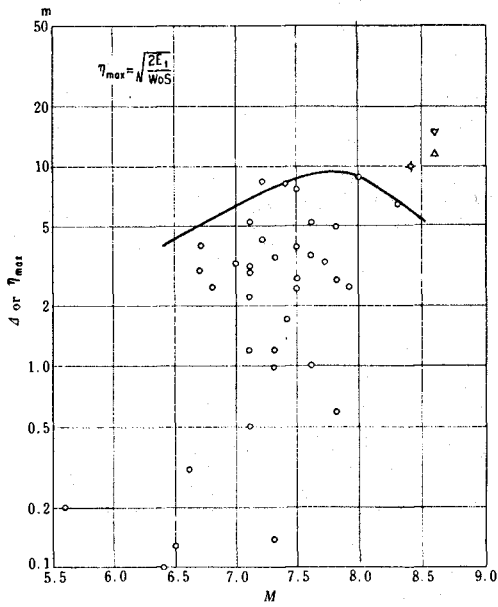


Fig.4 Relationship of Maximum Dislocation  $\eta_{max}$  to Earthquake Magnitude  $M$ .

Table 2

m	M	$E_t$ (ton-m)	a (km)	b (km)	$\eta_{\max}$ (m)
1	7.45	$1.000 \times 10^{11}$	32.61	27.35	8.534
2	7.85	$3.985 \times 10^{11}$	70.72	42.28	9.301
3	8.23	$1.585 \times 10^{12}$	202.00	89.77	7.535

In fig. 4 the relationship between the maximum dislocations  $\eta_{\max}$  and the earthquake magnitudes M thus computed is shown by a curve with plotted data of white circles given by Wilson for the resultants of maximum horizontal and vertical ground displacements  $d$ . Although they are not the same definition, our estimation is certified to give reasonable results for the design purpose. The maximum three points of M of 8.5 were obtained in the Mino-Owari earthquake in Japan (1891), Assam earthquake in India (1897) and the Alaskan earthquake in USA (1899). It seems curious that our estimation has the maximum dislocation of about 10 meters at the magnitude of 7.8, however the resulted maximum water elevation increases monotonously with the magnitude as shown afterwards.

#### NUMERICAL COMPUTATION SCHEME AND THE BOUNDARY CONDITIONS

Basic equations are;

$$\frac{\partial M}{\partial t} + \frac{M}{h+\zeta-\eta} \cdot \frac{\partial M}{\partial x} + \frac{N}{h+\zeta-\eta} \cdot \frac{\partial M}{\partial y} = -g(h + \zeta - \eta) \frac{\partial \zeta}{\partial x} - \frac{\tau_{bx}^*}{\rho_w} \quad (9)$$

$$\frac{\partial N}{\partial t} + \frac{M}{h+\zeta-\eta} \cdot \frac{\partial N}{\partial x} + \frac{N}{h+\zeta-\eta} \cdot \frac{\partial N}{\partial y} = -g(h + \zeta - \eta) \frac{\partial \zeta}{\partial y} - \frac{\tau_{by}^*}{\rho_w} \quad (10)$$

$$\frac{\partial \zeta}{\partial t} - \frac{\partial \eta}{\partial t} = - \left( \frac{\partial M}{\partial x} + \frac{\partial N}{\partial y} \right) \quad (11)$$

in which x, y are the horizontal orthogonal axis. The total depth H is the undisturbed water depth h plus the surface deviation  $\zeta$  minus the vertical upheaval of the sea bottom  $\eta$ , then

$$H = h + \zeta - \eta \quad (12)$$

In the long-period waves the velocity distributions along the vertical to the still water surface can be assumed uniform and are expressed by U and V for x and y directions. Then the volume flux per unit width are expressed by  $M=UH$  and  $N=VH$  respectively.

$\tau_{bx}^*$  and  $\tau_{by}^*$  are (x, y) components of the bottom friction and are expressed by

$$\vec{\tau}_b = \rho_w \gamma_b^2 \mathbf{V} | \mathbf{V} | \quad (13)$$

where  $\mathbf{V}$  is the velocity vectors,  $\rho_w$  is the density of water and  $\gamma_b^2$  is

the friction factor and is taken as  $2.6 \times 10^{-3}$  c.g.s. tentatively.

Procedures to make up the finite-difference schemes are basically the same proposed by Dr. Hino and not described here (1972)<sup>6)</sup>. Discharge flux M and N and water levels  $\zeta$  are computed at different grid points shown in fig. 5 in a staggered scheme, which computations are alternative in the time step  $\Delta t$ .

Fig. 6 shows the schematic domain to be calculated. ABOCD is the boundary in the sea and DEA is the coastal boundary. In deep sea linear long waves of negligible amplitude can be assumed, then characteristics are derived for progressive and retrogressive waves following to Dr. Kajiura<sup>7)</sup>,

$$z^{\pm} = \frac{Q}{bc} \pm \zeta = \text{const} \quad (14)$$

in which c is the wave celerity and b is the breadth. Eq.(14) can be transformed as

$$\begin{aligned} \text{for the positive x direction} & \quad \frac{M}{c} + \zeta = z_{M+} \\ \text{for the negative x direction} & \quad \frac{M}{c} - \zeta = z_{M-} \\ \text{for the positive y direction} & \quad \frac{N}{c} + \zeta = z_{N+} \\ \text{for the negative y direction} & \quad \frac{N}{c} - \zeta = z_{N-} \end{aligned} \quad (15)$$

If there is no wave invading from outside,

$$\text{on the boundary AB, } N=0 \quad \text{and} \quad z_{M-} = 0 \quad \text{then, } M=c\zeta$$

$$\text{on the boundary OC, } N=0 \quad \text{and} \quad z_{M+} = 0 \quad \text{then, } M=-c\zeta$$

$$\text{on the boundary OB, } M=0 \quad \text{and} \quad z_{N+} = 0, \quad \text{then } N=-c\zeta$$

$$\text{on the boundary CD, } M=0 \quad \text{and} \quad z_{N-} = 0, \quad \text{then } N=c\zeta$$

The values of  $\zeta$  or M and N at points just one step outside of the boundary are assumed to propagate from points on the boundary with the celerity of long waves.

On the coastal boundary, only normal component of discharge flux is assumed zero but parallel component is not. Then there are 12 kinds of coastal boundary conditions.

Fig. 7 shows the computed domain in which the south coast of Hokkaido, the Sanriku Coast and the Japan Submarine Trench are included. The coastal boundary was simulated by the zigzag grid line and depth in front of it was assumed as that of just one step inside grid points. The space difference DS was 24 kilometers and time difference DT was 30 seconds. Instability was not experienced and smoothing technique was not employed.

#### EFFECTS OF THE UPHEAVE VELOCITY OF THE SEA BED

Numerical tests were performed to investigate effects of upheave velocity of the sea bed upon the configurations in near coast offshore

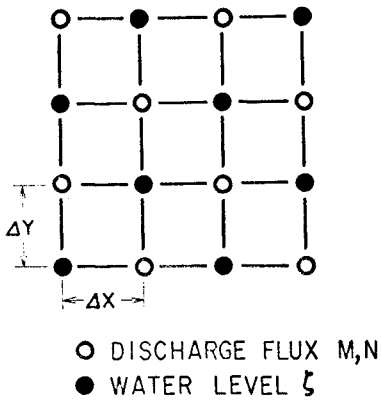


Fig.5 Schematic Grid Points

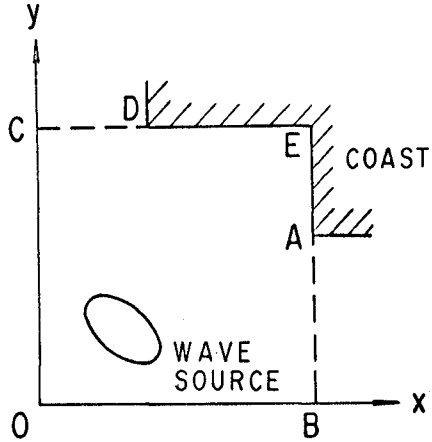


Fig.6 Schematic Domain

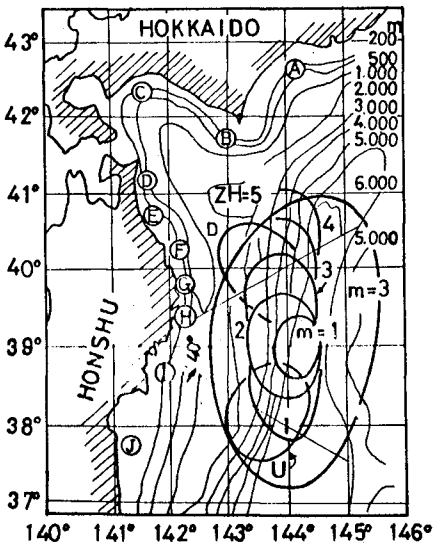


Fig.7 The Computed domain

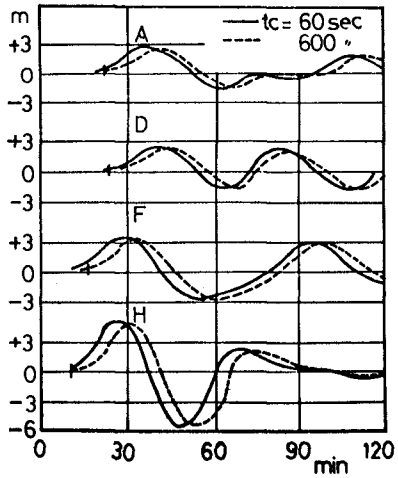


Fig.8 Effects of the upheave velocity of the Sea Bed.

region. For this purpose the source area for the tsunami magnitude  $m$  of 3 which dimension is given in table 2 is set as shown in fig.7. The maximum upheaval  $\eta_{\max}$  was constant as 5.19 meters because of the feasibility of the time spacing. The duration times to this maximum upthrust  $t_c$  were changed as five kinds such as 60, 90, 210, 300 and 600 secs in which the velocity of the bed movement was constant.

Fig.8 shows computed wave profiles at the grid points just one step inside from the coastal boundary where the depths were about 200 meters as shown by points of A, D, F and H in fig.7. Only two extreme cases are shown here such that  $t_c$  are 60 and 600 secs.

Hammack and Raichlen defined the disturbance time-size ratio by  $t_c \cdot \sqrt{gh}/b$  in which  $b$  was the half-length of the breadth of the disturbance in the direction of the wave propagation, which was assumed in this case as that of the minor axis, that was 90 kilometers.<sup>(7)</sup>  $h$  was given by the mean depth of the source which was 4925 meters along the minor axis. Then values of this no-dimensional ratio are between 0.147 and 1.471. Due to Hammack and Raichlen, such movements are classified as impulsive bed deformation and the ratio of the maximum wave heights thus generated  $\zeta_{\max}$  and the maximum upheaval  $\eta_{\max}$  is constant. As shown in fig.8, two configurations are almost same at each point except the difference of the arrival time which support the theory of Hammack and Raichlen and make our attempt somewhat easier.

#### COMPARISON OF WAVE CONFIGURATIONS AT PERIPHERAL POINTS AND THOSE IN NEAR-COAST OFFSHORE REGION

Fig.9 shows the tsunami waves at the peripheral point on the major axis  $P_{6-11}$  and at the nearest offshore point A calculated for the wave source of  $m$  of 3. Also in fig.10, those at the peripheral point on the minor axis  $P_{10-21}$  and at the point 1 are compared.

At the peripheral points, abrupt water rises are shown followed by oscillations which periods are about 10 minutes on the major axis and 15 minutes on the minor axis each. However at the near-coast offshore points, very slow undulations with the periods of about 70 minutes are computed. However such period was not observed at the Sanriku Large Tsunami of 1933 when the periods were reported as 10 to 20 minutes.

The Ursell numbers are computed following the proposal by Hammack and Raichlen such as,

$$U = \zeta_0^3 / h^3 \|\zeta_x\|^2 \quad (17)$$

, in which  $U$  is the Ursell number,  $\zeta_0$  is the maximum water rise and  $\zeta_x$  is the space derivative on the first wave and is computed by the maximum time derivative divided by the long wave celerity  $c$  ( $=\sqrt{gh}$ ). Then at  $P_{6-11}$ ,  $U = 8.7 \times 10^{-4}$  and at A,  $U=860$ . This means the waves are linear under frequency dispersion process at the peripheral points, but are finite and non-linear under amplitude dispersion process at the near-coast offshore points. Hammack and Raichlen had pointed that soliton formation might be expected for the Ursell number of the order 1. However Galvin had reported three solitons for the Ursell number of 100 to 500 (1972), which had been supported by the numerical experiments by Tsuchiya-Yamada (1973).<sup>(8)(9)</sup> So such soliton formation is expected on the tsunami propagation from the peripheral to the coast. The space grids were too coarse to make realize such dispersion. If the wave could be dispersed into three solitons as pointed by Galvin and Tsuchiya-Yasuda,

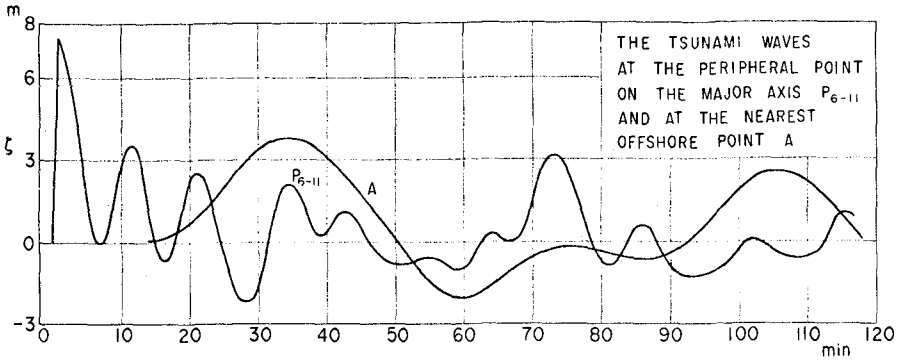


Fig.9 Comparison of Wave Configurations at Peripheral Points and those in Near-coast Offshore Region

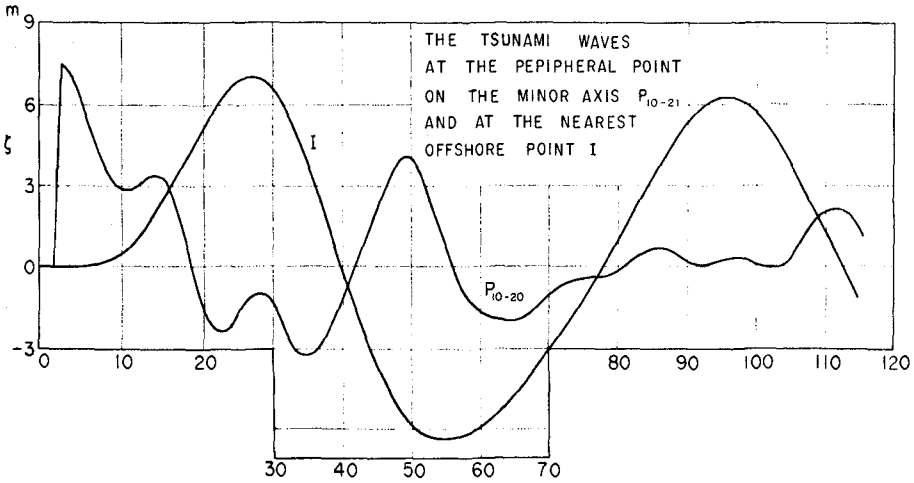


Fig.10 Comparison of Wave Configurations at Peripheral Points and those in Near-coast Offshore Region

the period might be about 20 minutes which should support observations.

#### EFFECTS OF THE TSUNAMI MAGNITUDES

To investigate effects of the tsunami magnitudes upon the wave heights in near-coast offshore region, numerical tests were carried out for the wave sources with different magnitude. Their centers and two axis are coincided with each other. As mentioned above, the bed deformation is impulsive. So the duration time of the bed upheaval was taken as constant of 60 seconds.

Fig. 11 is an example. In fig.12, the white circles are plotted by the first maxima in fig. 11. As these waves are stopped by the vertical wall with perfect reflection, the heights of the stationary waves will be double to them which were plotted in triangles. The straight line is given by the following equation of Wilson,

$$\log_{10} \zeta_{\max} = 0.75 M - 5.07 \quad (18)$$

The curve was presented by Iwasaki (1973).<sup>00</sup> Then the doubled maxima are rather closely forecasted by Wilson's formula.

The arrival time of the long wave to the point which distance from the peripheral point is  $X'$  may be approximated by  $X'/\sqrt{gh'}$ , where  $\bar{h}$  is the mean depth along the path. The toe of the rising limb appeared rather earlier than this time.

In fig. 13, no-dimensional time difference between  $X'/\sqrt{gh'}$  and the arrival time of the first maximum  $t_{\max}$  as computed by

$$T_{\max} = t_{\max} \cdot \sqrt{\frac{g}{h}} - \frac{X'}{h} \quad (19)$$

is taken as the ordinate and  $X'/h$  is taken as the abscissa. It is found that in the case of the magnitude of 3 the first maxima get retarded from the front more and more as the travel distance increases. This is contrary to the prediction by the finite amplitude long wave theory, which shows clearly the effects of dispersion. However in cases of the magnitudes of 2 and 1, such retardation gets restored for the increase of the travel distance.

In fig. 14, the ratios of the maximum wave amplitudes and the maximum ground upheavals  $\zeta_{\max}/\eta_{\max}$  are plotted against the no-dimensional travel distances  $X'/\bar{h}$ . Clearly these ratios decrease with the travel distance and approach to constant values when  $X'/\bar{h}$  is larger than 200. Points F, G, H and I are off the Sanriku Coast with nearly the same distance to the source. However values of  $\zeta_{\max}/\eta_{\max}$  at these points are remarkably scattered with each other which may be attributed to the effects of the local bottom topography.

#### EFFECTS OF THE SOURCE LOCATIONS

As shown in fig.7, five source areas of the magnitude of 2 were set so that their major axes are coincided to the same meridian line but their centers are shifted along it. Such models are called as ZH 1, ZH 2, ..., ZH 5. Results are shown in fig. 15-18 in which waves are drawn so as the times when the first waves get back to the undisturbed level to coincide with each other. As shown in them, the first wave configurations at each point are not so sensitive with the variation of the

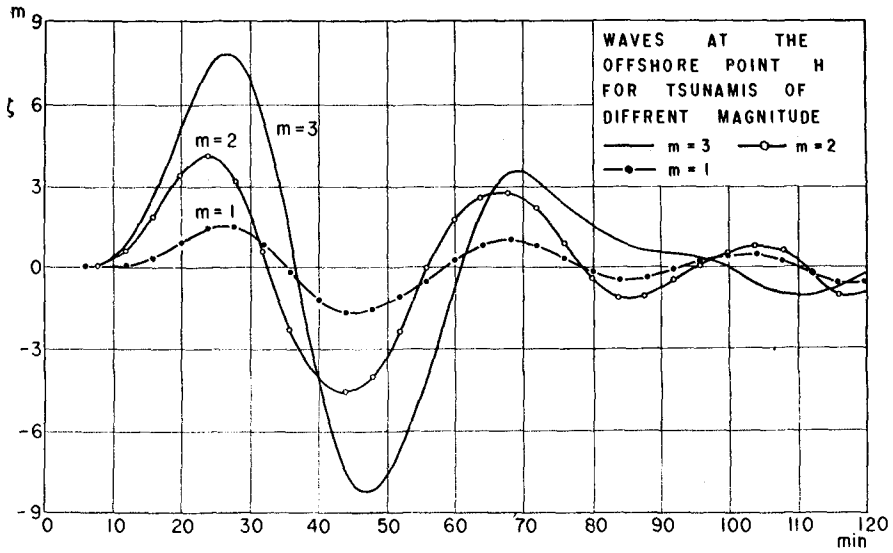


Fig.11 Effects of the Tsunami Magnitudes

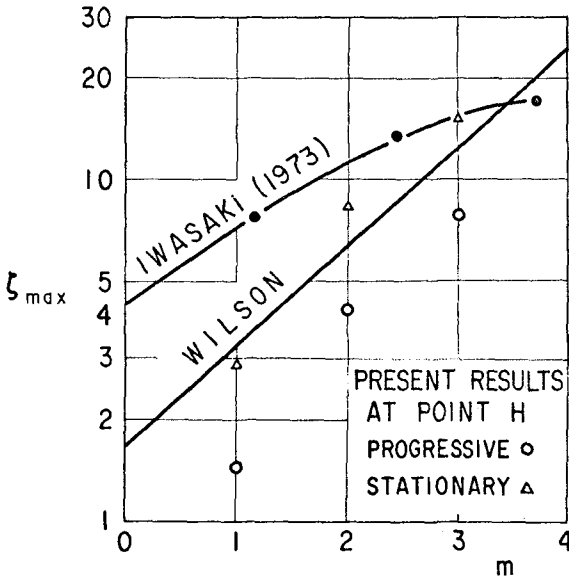


Fig.12 Relationship of the Maximum Amplitudes to the Tsunami Magnitudes

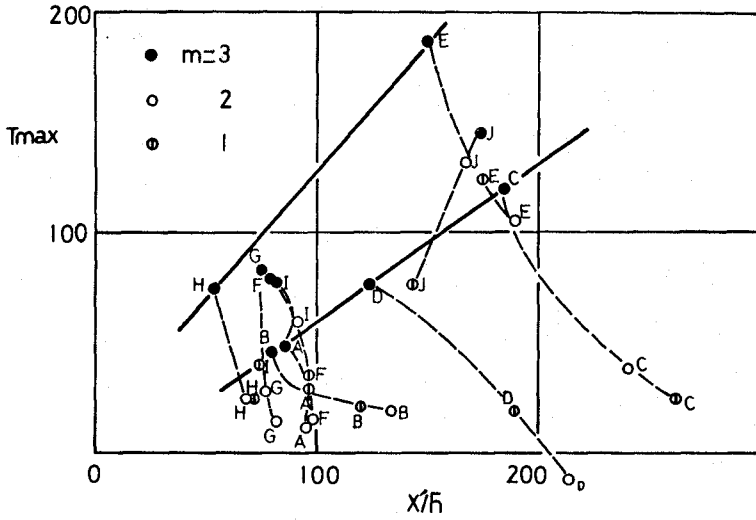


Fig.13 Relationship of  $T_{max}$  to  $X'/h$

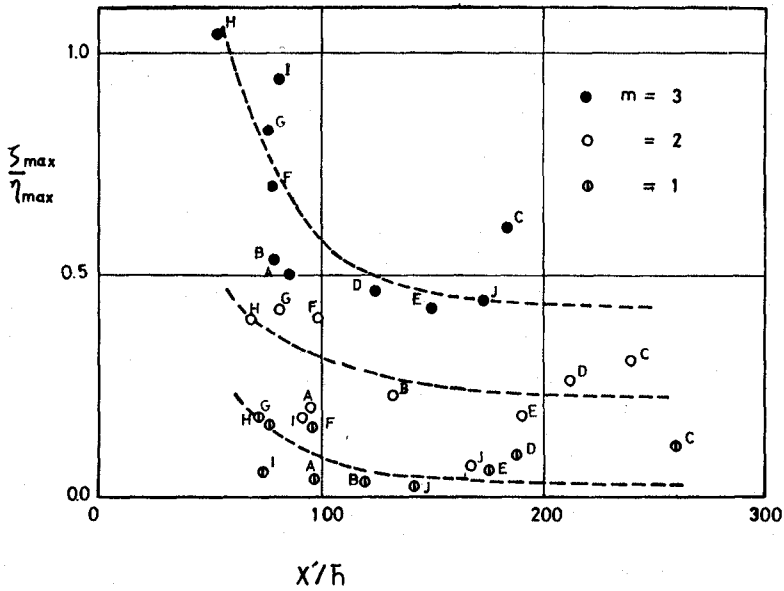


Fig.14 Relationship of  $\zeta_{max}/\eta_{max}$  to  $X'/h$

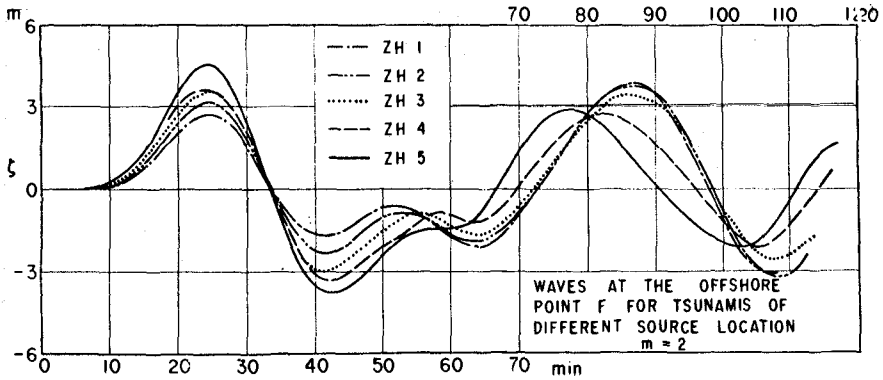


Fig.15 Effects of the Source Location at Point F

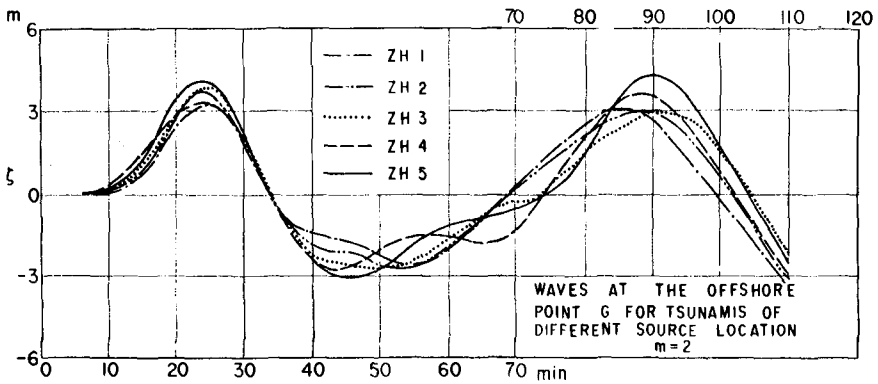


Fig.16 Effects of the Source Location at Point G

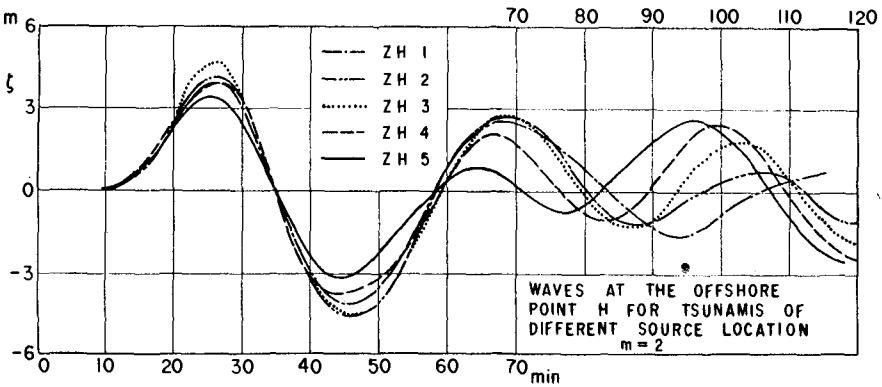


Fig.17 Effects of the Source Location at Point H

center location, but are very much unique at each points. This result is important for the design purpose and stresses the inevitable necessity of the numerical model tests.

#### EFFECTS OF DIRECTION OF THE INCIDENT WAVES

Lastly three models were tested to investigate effects of direction of the incident waves. As shown in fig. 7, the wave source of which the direction of the minor axis is normal to the coast is called as PZC and that of which the axis direction is 20 degrees northward to PZC is called as PZU. Also the wave source of which the minor axis is rotated 20 degrees southward to PZC is called as PZD.

Results are shown in fig.19-22. In every case, the tsunami magnitude is 2. At the point F, PZU gives the highest wave as this source approaches to F most closely. Same result is obtained at the point I where PZD gives the highest. At G and H, the wave source PZC gives the maximum, which is in accord to the common sense.

#### CONCLUSIONS

Near-coast offshore wave forms along the Sanriku and the southern coast of Hokkaido are obtained by the numerical computations with the tsunami source models of three kinds of magnitude set on the western slope to the Japan Submarine Trench. Conclusions thus obtained are as follows;

1. The dimensions of the source areas are reasonably estimated by eqs. (1) to (7).
2. Computation scheme and the boundary conditions discussed here make possible the computation of tsunami waves.
3. If the tsunami magnitudes are between 1 and 3 and the wave sources are located such that shown in this paper, sea bed movement can be classified as impulsive bed deformation. So the deformation velocity can be assumed tentatively. Computed configurations in near-coast offshore region are not sensitive to this and are decided by the maximum upheaval.
4. At the peripheral points of the wave source, abrupt water rises are shown followed by oscillations with periods of 10 to 15 minutes for the tsunami magnitude of 3. However very slow undulations with period of about 70 minutes are computed in the near-coast offshore region. This should be checked by the investigation of the soliton formation in the future.
5. The first maxima at the vertical cliff nearest to the source can be approximated by Wilson's empirical equation. When  $m=3$ , the first maxima get retarded from the front more and more as the travel distance increases. However when  $m=2$  and 1, such retardation gets restored with the travel distance.

Variation of the first maxima due to locality is remarkable in the range of  $X'/h$  smaller than 100.

6. The first wave configurations are not so sensible to the variation of the center location of the wave source, if their major axes are on the same meridian line and the variation is confined to the extent treated in this paper.
7. The highest wave is obtained when the minor axis of the wave source

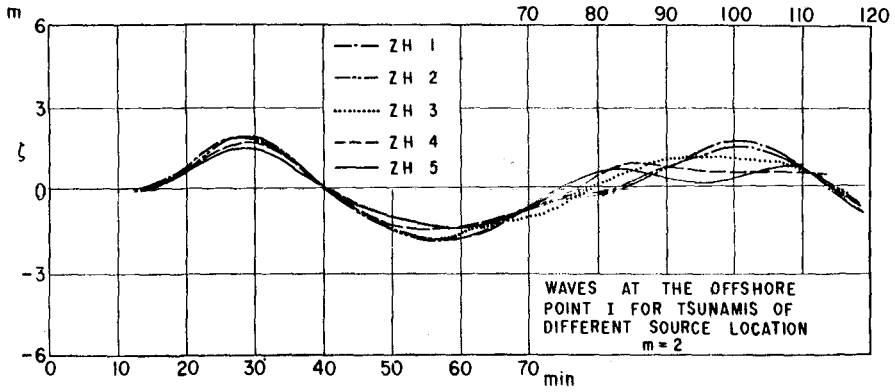


Fig.18 Effects of the Source Locations at Point I

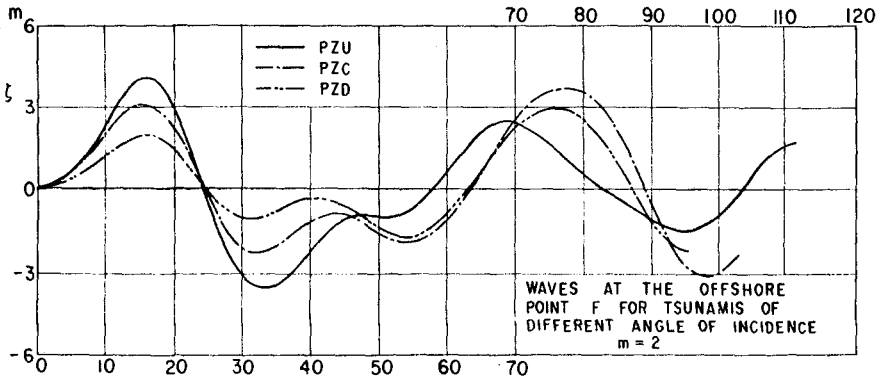


Fig.19 Effects of the Direction of the Incident Waves at Point F

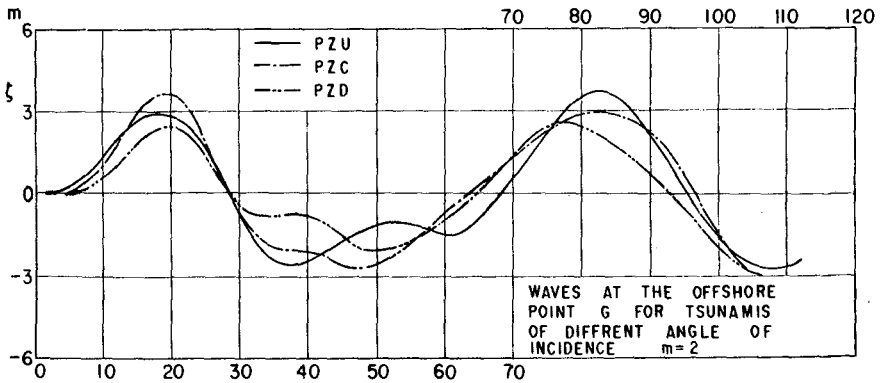


Fig.20 Effects of the Direction of the Incident Waves at Point G

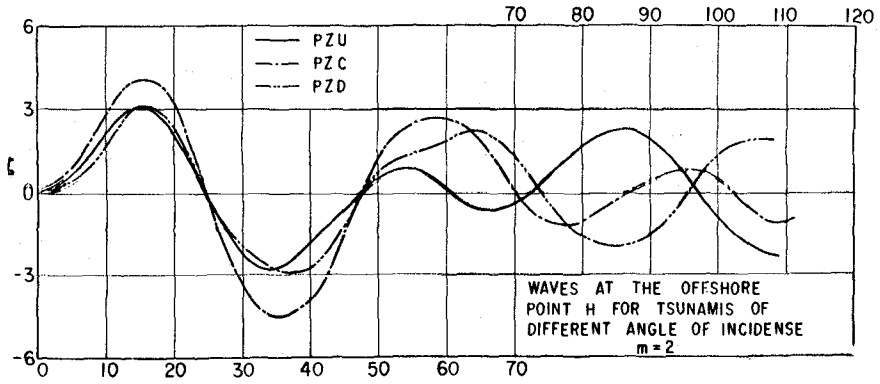


Fig.21 Effects of the Direction of the Incident Waves at Point H

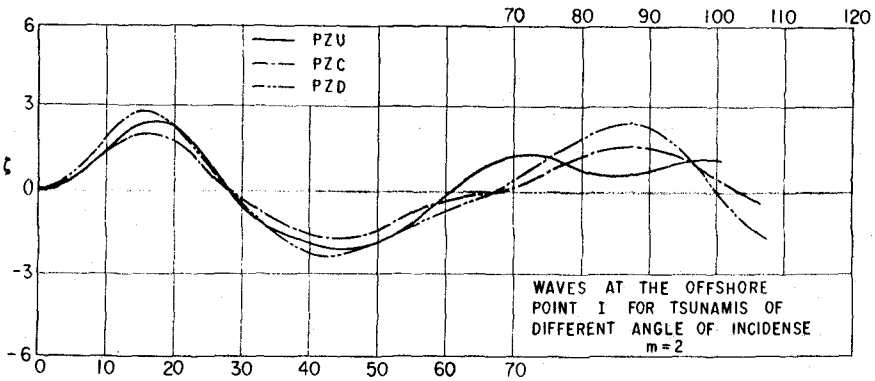


Fig.22 Effects of the Direction of the Incident Waves at Point I

is normal to the coast line, or when the source area gets closest to the coast.

## ACKNOWLEDGEMENTS

The author would like to express his appreciation to Mr. Tzemin Yang for his excellent achievements of the numerical computations.

## REFERENCE

- 1) K. Iida, "Magnitude of Tsunamigenic Earthquake, Aftershock Area, And Area of Tsunami Origin." Geophysical Papers dedicated to Professor Kenzo Sassa. (1963)
- 2) T. Hatori, "Dimensions and Geographic Distribution of Tsunami Sources near Japan." B.E.R.I. vol.47 (1969)
- 3) K. Iida, "Earthquake Energy and Earthquake Fault" J. Earth Sci., Nagoya Univ. vol.7(2) (1959)
- 4) B. Wilson, "The Nature of Tsunamis, their Generation and Dispersion in Water of Finite Depth." NESCO Tech. Report No. SN 57-2 (1962)
- 5) R. Takahashi, "Potential Tsunami Inundation Along Japan Sea Coast. B.E.R.I. vol.28 (1950)
- 6) M. Hino, "Fluid Analysis (I)" Proc. ASCE vol.57 (1972)
- 7) J.L. Hammack, F. Raichlen, "Tsunamis-A Model of their Generation and Propagation." C.I.T. Report No. KH-R-28 (1972)
- 8) C.J. Galvin, "Wave breaking in Shallow Water. Waves on Beaches and Resulting Sediment Transport. edited by R.E. Meyer, Academic Press (1972)
- 9) Y. Tsuchiya, T. Yasuda, "Wave Transformation in Shallow Water - On the Generation of Solitons" Proc. 20th Interine Coastal Engineering (1973) (in Japanese)
- 10) T. Iwasaki, "The Wave Sources of the Designed Tsunamis" Prof. 20th Interine Coastal Engineering (1973) (in Japanese)

